Adaptive State Space Control of a Camera Platform for an Autonomous Ground Vehicle

Alois Unterholzner and Hans-Joachim Wünsche

***Abstract*—A novel multi-focal camera vision system for autonomous ground vehicles is presented. The camera platform is pivotable in pitch and yaw axis to provide a wide field of view. Camera configuration of yaw axis can be changed while retaining camera calibration for later reuse. But different configurations are likely to result in different system dynamics, which implies the need for a motion controller capable of adapting to distinct configurations. This paper presents a brief description of the platform design. Furthermore the design of the adaptive platform control law is presented together with experimental results to demonstrate the validity of the approach.**

I. Introduction

Perception of the environment is an important prerequisite for autonomous ground vehicles to be able e.g. to distinguish drivable from impassable terrain, to avoid obstacles and to navigate within its environment. Visual data is one important source of information for the perceptional system. For autonomous ground vehicles visual sensors should be able to meet – possibly competing – requirements such as wide field of view, high resolution and stereo vision. A wide field of view is desirable to scan simultaneously as much of the vehicles environment as possible. A high resolution is required for early detection of distant objects. The maximum range of object detection limits the maximum speed of the vehicle. Stereo vision is used to gather 3D information of the environment. These requirements and the resulting design of multi focal camera platforms are discussed e.g. in [1] and [2]. According to [1], platforms pivotable in pitch and yaw axis and equipped with several cameras, that either provide a wide field of view or a high resolution, offer a good compromise to meet the needs of visual perception in autonomous ground vehicles. An overview on camera platforms, especially platforms for humanoid robots, is given in [3] and [4]. The design of motion controllers for camera platforms in autonomous ground vehicles is discussed in [5].

Although a camera platform offers a good compromise covering more or less the needs of each visual perception module of the autonomous vehicle, the optimal camera configuration for a single perception module can differ from the currently utilized platform configuration. To detect e.g. lane markings black/white cameras might be best, to detect drivable areas in off-road terrain color cameras might be better. Divergent cameras offer a wide field of view. Parallel cameras, on the contrary, increase the range where stereo vision is possible. Depending on their range of interest different perception modules require different focal lengths of camera lenses. Therefore the software designer prefers to use the camera configuration that suits best his application's demands. For this reason, in our research group the camera platform configuration of our experimental vehicle is frequently changed.

The authors gratefully acknowledge partial support of this work by the Deutsche Forschungsgemeinschaft (German Research Foundation) within the Transregional Collaborative Research Centre 28 *Cognitive Automobiles*.

All authors are with the Institute for Autonomous Systems Technology (TAS), University of the Bundeswehr Munich, 85577 Neubiberg, Germany. Contact author email: alois.unterholzner@unibw.de

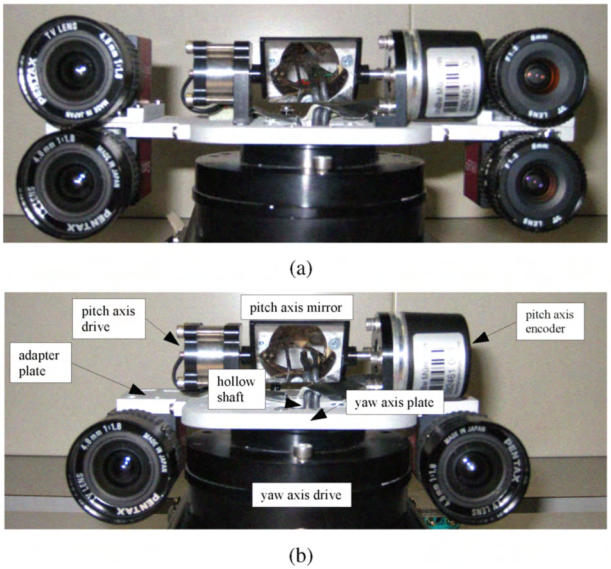

Fig. 1. Two possible camera platform configurations

With every change of the cameras the extrinsic camera parameters are lost and recalibration is required. Moreover exchanging cameras may alter platform dynamics due to different camera masses, which in turn alters platform inertia leading to reduced performance of platform motion.

To overcome these problems we developed a camera platform following not only the design recommendations given in [1], but offering additionally the possibility to exchange cameras while retaining camera calibration for later reuse of this configuration. Two possible platform configurations are shown in Figure 1. For easy exchange of the cameras they are mounted on adapter plates (Fig. 1(b)). These plates are attached to the platform yaw axis plate. For high repeat accuracy the plates are positioned with adjust pins relative to the yaw axis plate. Thus camera calibration is preserved as long as the cameras remain fixed to the adapter plates. Pitch axis drive and position sensor are mounted on top of the yaw axis plate. The pitch axis camera is placed in the hollow shaft of the yaw axis drive. A mirror is used to reflect the horizontal view towards the camera in the hollow shaft. Inertia of the pitch axis is kept low this way since only the mirror has to

978-1-4244-3504-3/09/$25.00 ©2009 IEEE

be rotated. Thus the weight of the pitch axis drive can also be kept to a minimum, which in turn reduces inertia of the yaw axis. Placing the pitch axis camera in the centre of rotation of the yaw axis further reduces yaw axis inertia.

But, as already mentioned, altering the camera configuration may lead to a change in platform dynamics, which is obvious from Figure 1(a) and 1(b). Therefore this paper presents an adaptive motion controller capable of adjusting to different camera configurations. The following parts of the paper are organized as follows: In section II the dynamic model of platform yaw axis is derived. Section III presents the applied parameter estimator. Since we use state space control, in section IV the applied state estimator is introduced. The control law is derived in section V. Stability considerations are presented in section VI. Experimental results are discussed in section VII. Finally the paper concludes in section VIII.

II. Dynamic Model

Plant dynamcis can be modelled as a nonlinear second order differential equation:

$$(J_p + J_c) \cdot \ddot{\varphi} = k_m \cdot I - \tau_\varphi - \tau_{\dot{\varphi}} \tag{1}$$

with I as torque generating motor current, k_m motor torque constant, J_p inertia of platform yaw axis and J_c inertia resulting from attached cameras including adapter plates. The angular velocity dependent disturbance torque $\tau_{\dot{\varphi}}$ is described by

$$\tau_{\dot{\varphi}} = \tau_c \cdot sgn(\dot{\varphi}) + d \cdot \dot{\varphi} \tag{2}$$

with τ_c representing Coulomb and d viscous friction coefficient, and $sgn(x)$ being the signum function. The angular position dependent disturbance torque

$$\tau_\varphi = r \cdot m \cdot g \cdot sin(\theta_p) \cdot cos(\varphi) \tag{3}$$

results from unbalanced mass m of platform yaw axis, with distance r from center of gravity of unbalanced mass m to center of rotation of platform yaw axis, g gravitational acceleration and θ_p adjustable pitch angle of platform yaw axis. Unbalanced mass results from pitch axis encoder outweighing pitch axis drive (Fig. 1(b)) and from the mass of the cameras attached to one side of the platform outweighing camera mass of the opposite side (Fig. 1(a)). Defining $r \cdot m \cdot g \cdot sin(\theta_p) =: \tau_u$ disturbance torque τ_φ can be written as

$$\tau_\varphi = \tau_u \cdot cos(\varphi) \tag{4}$$

With equations (2) and (4) plant dynamics (1) can be summarized to

$$J \cdot \ddot{\varphi} = k_m \cdot I - d \cdot \dot{\varphi} - \tau_c \cdot sgn(\dot{\varphi}) - \tau_u \cdot cos(\varphi) \tag{5}$$

III. Parameter Estimation

Since model parameters J, d, τ_c and τ_u are unknown a parameter estimator is used to get estimates $\hat{J}$, $\hat{d}$, $\hat{\tau}_c$ and $\hat{\tau}_u$ respectively. Thus discretizing equation (5) using forward differences as suggested in [6]

$$\begin{aligned} \dot{\varphi} &= (\varphi_{k+1} - \varphi_k)/T \\ \ddot{\varphi} &= (\varphi_{k+2} - 2\varphi_{k+1} + \varphi_k)/T^2 \end{aligned} \tag{6}$$

we derive a discrete time plant model

$$\begin{aligned} \varphi_k &= -a_1 \cdot \varphi_{k-1} - a_2 \cdot \varphi_{k-2} + b_2 \cdot I_{k-2} \\ &\quad -\delta_1 \cdot sgn(\frac{\varphi_{k-1} - \varphi_{k-2}}{T}) - \delta_2 \cdot cos(\varphi_{k-2}) \end{aligned} \tag{7}$$

with parameters

$$\begin{aligned} a_1 &= \tfrac{Td}{J} - 2, \quad a_2 = 1 - \tfrac{Td}{J}, \quad b_2 = \tfrac{k_m T^2}{J} \\ \delta_1 &= \tfrac{\tau_c T^2}{J}, \quad \delta_2 = \tfrac{\tau_u T^2}{J} \end{aligned} \tag{8}$$

which is linear in the parameters. Thus (7) can be written as linear regression

$$\varphi_k = \phi_{k-1}^T \theta_{k-1} \tag{9}$$

with regression variables

$$\begin{aligned} \phi_{k-1} &= (-\varphi_{k-1}, \ -\varphi_{k-2}, \ I_{k-2}, \\ &\quad sgn\left((\varphi_{k-1} - \varphi_{k-2})/T\right), \ cos(\varphi_{k-2}))^T \end{aligned} \tag{10}$$

and time variable parameter vector

$$\theta_{k-1} = (a_{1_{k-1}}, \ a_{2_{k-1}}, \ b_{2_{k-1}}, \ \delta_{1_{k-1}}, \ \delta_{2_{k-1}})^T \tag{11}$$

suitable for a discrete time Recursive Least Squares (RLS) type parameter estimation scheme

$$\begin{aligned} K_{\theta_k} &= \frac{P_{\theta_{k-2}} \phi_{k-1}}{1 + \phi_{k-1}^T P_{\theta_{k-2}} \phi_{k-1}} \\ \bar{P}_{\theta_{k-1}} &= P_{\theta_{k-2}} - \frac{P_{\theta_{k-2}} \phi_{k-1} \phi_{k-1}^T P_{\theta_{k-2}}}{1 + \phi_{k-1}^T P_{\theta_{k-2}} \phi_{k-1}} \\ \hat{\theta}_k &= \hat{\theta}_{k-1} + K_{\theta_k} \left(\varphi_k - \phi_{k-1}^T \hat{\theta}_{k-1}\right) \end{aligned} \tag{12}$$

as described in [7]. $\bar{P}_{\theta_{k-1}}$ in (12) tends to zero for $k \to \infty$ and therefore estimator gain K_{θ_k} also tends towards zero. Parameter estimates are then not updated any longer: The estimator is virtually switched off. In order to be able to track time varying parameters, $\bar{P}_{\theta_{k-1}}$ must be kept away from zero.

To track slowly time varying (drifting) parameters we use covariance modification

$$P_{\theta_{k-1}} = \bar{P}_{\theta_{k-1}} + Q_{\theta_{k-1}} \tag{13}$$

as suggested in [7] to keep $\bar{P}_{\theta_{k-1}}$ away from zero. The underlying assumption of equation (13) is a random walk model

$$\hat{\theta}_k = \hat{\theta}_{k-1} + w_{k-1} \tag{14}$$

for parameter variation, where w_{k-1} is a white noise sequence having covariance matrix $Q_{\theta_{k-1}}$. To avoid estimator windup with $P_{\theta_{k-1}}$ growing unbounded due to estimation data being not persistently exciting for a long time period, $trace(P_{\theta_{k-1}})$ is monitored and $Q_{\theta_{k-1}}$ is set to zero for $trace(P_{\theta_{k-1}})$ exceeding a certain threshold. To track fast parameter changes (jump parameters) covariance resetting is used (from [7]). Setting

$$P_{\theta_{k-1}} = \alpha I, \quad 0 < \alpha_{min} \leq \alpha \leq \alpha_{max} < \infty \tag{15}$$

in case of a sudden increase of estimation error

$$\epsilon_k = \varphi_k - \phi_{k-1}^T \hat{\theta}_{k-1} \tag{16}$$

indicating an abrupt parameter change, the parameter estimator is reinitialized with a large error covariance and therefore able to track fast parameter changes.

To further enhance the robustness of parameter estimation and to be able to include prior knowledge about the parameters, we use parameter projection to constrain parameter estimates to stay within

$$\theta_{min}(i) \;\leq\; \hat{\theta}(i) \;\leq \theta_{max}(i), \quad \forall\, i \tag{17}$$

We use the parameter projection scheme described in [7], which retains convergence properties of algorithm (12) to (15). The constrained parameters are derived as follows

$$\hat{\theta}_k' = \hat{\theta}_k + P_{\theta_{k-1}} S_k (S_k^T P_{\theta_{k-1}} S_k)^{-1} S_k^T (\theta_c - \hat{\theta}_k) \tag{18}$$

with θ_c being the vector of constrained parameters defined as

$$\theta_c(i) = \begin{cases} \theta_{max}(i) & \text{for } \hat{\theta}(i) > \theta_{max}(i) \\ \theta_{min}(i) & \text{for } \hat{\theta}(i) < \theta_{min}(i) \\ \hat{\theta}(i) & \text{else} \end{cases}, \quad \forall i \tag{19}$$

Matrix S is used to select only those parameters for projection that are not satisfying equation (17). S is built by adding unit vectors e_i to S if $\hat{\theta}(i)$ is not within constraints.

Since $\hat{\theta}(i)$ may be a function of more then one plant parameter (cf. eq. 8), deriving $\theta_c(i)$ from upper and lower bounds of estimated plant parameters

$$p_{min}(j) \;\leq\; \hat{p}(j) \;\leq p_{max}(j), \quad \forall\, j \tag{20}$$

with vector of estimated plant parameters

$$\hat{p} = (\hat{J}, \hat{d}, \hat{\tau}_c, \hat{\tau}_u)^T \tag{21}$$

is not straightforward. Therefore we calculate θ_c at every time instant k. If $\hat{p}(j)$ is not within the limits of (20) we change plant parameter bounds as follows

$$\begin{aligned} p_{min_k}(j) &= p_{max_k}(j) \text{ for } \hat{p}_k(j) > p_{max_k}(j) \\ p_{max_k}(j) &= p_{min_k}(j) \text{ for } \hat{p}_k(j) < p_{min_k}(j) \end{aligned} \tag{22}$$

Otherwise they are left unchanged. Then we use equation (8) to calculate $\theta(i)$ for all 2^j combinations of $p_{min_k}(j)$ and $p_{max_k}(j)$ setting the bounds of θ to

$$\theta_{max_k}(i) = \max_{2^j} \theta(i,j) \text{ and } \theta_{min_k}(i) = \min_{2^j} \theta(i,j) \tag{23}$$

IV. State Estimation

For applying a state space control law full state information is required. Since only the yaw axis position is measured, we need a state estimator to derive full state information. Since the plant model (5) is nonlinear, we use parameter estimates $\hat{\tau}_c$ and $\hat{\tau}_u$ to compensate for the nonlinear disturbance terms in equation (5) with disturbance feed forward

$$I_{ff} = k_m^{-1} \cdot (\hat{\tau}_c \cdot sgn(\dot{\varphi}) + \hat{\tau}_u \cdot cos(\varphi)) \tag{24}$$

In [6] a similar approach is suggested for adaptive friction compensation. The plant input current I can be written as follows:

$$I = I_{ff} + I_{fb} + I_{ref} \tag{25}$$

with I_{ff} resulting from feedforward control, I_{fb} resulting from feedback control and I_{ref} resulting from reference input r. Inserting feedforward control (24) in the plant model (5) we get

$$\begin{aligned} J \cdot \ddot{\varphi} \;=\; & k_m \cdot (I_{fb} + I_{ref}) - d \cdot \dot{\varphi} \\ & -(\tau_c - \hat{\tau}_c) \cdot sgn(\dot{\varphi}) - (\tau_u - \hat{\tau}_u) \cdot cos(\varphi) \end{aligned} \tag{26}$$

Summarizing the remaining disturbance torques resulting from parameter estimation errors $\tau_u - \hat{\tau}_u$ and $\tau_c - \hat{\tau}_c$ as well as from unmodelled disturbances in one disturbance torque τ_d, equation (26) can be written as

$$J \cdot \ddot{\varphi} = k_m \cdot (I_{fb} + I_{ref}) - d \cdot \dot{\varphi} - \tau_d \tag{27}$$

We use

$$\ddot{\tau}_d = 0 \tag{28}$$

as disturbance model, as this is found in [8] to be a good compromise between model complexity and estimation accuracy in the context of friction compensation.

Now we are able to derive an state estimator. Using continuous time state space formulation

$$\begin{aligned} \dot{x} &= Fx + G\bar{u},\; y = Cx, \quad \text{with} \\ x &= (\varphi,\; \dot{\varphi},\; \tau_d,\; \dot{\tau}_d)^T,\; \bar{u} = I_{fb} + I_{ref} \end{aligned} \tag{29}$$

we derive from equation (27) and disturbance model (28) the state space description

$$\begin{aligned} F &= \begin{pmatrix} 0 & 1 & 0 & 0 \\ 0 & -\frac{d}{J} & -\frac{1}{J} & 0 \\ 0 & 0 & 0 & 1 \\ 0 & 0 & 0 & 0 \end{pmatrix},\; G = \begin{pmatrix} 0 \\ \frac{k_m}{J} \\ 0 \\ 0 \end{pmatrix}, \\ C &= (1,\; 0,\; 0,\; 0) \end{aligned} \tag{30}$$

As we are using a discrete time Kalman filter for state estimation we need a discrete time description of (30):

$$x_{k+1} = Ax_k + B\bar{u}_k,\; y_k = Cx_k \tag{31}$$

Using (6) for discretization we get

$$\begin{aligned} A &= \begin{pmatrix} 1 & T & 0 & 0 \\ 0 & \frac{J-Td}{J} & -\frac{T}{J} & 0 \\ 0 & 0 & 1 & T \\ 0 & 0 & 0 & 1 \end{pmatrix},\; B = \begin{pmatrix} 0 \\ \frac{k_m T}{J} \\ 0 \\ 0 \end{pmatrix} \\ C &= (1,\; 0,\; 0,\; 0) \end{aligned} \tag{32}$$

Replacing parameters J and d at every time step k with their estimates $\hat{J}_k$ and $\hat{d}_k$, we get $\hat{A}_k$ and $\hat{B}_k$ as state and input matrices respectively. Inserting these matrices in the Kalman filter equations

$$\begin{aligned} K_{s_k} &= \hat{A}_k P_{s_k} C^T (C P_{s_k} C^T + R_s)^{-1} \\ \hat{x}_{k+1} &= (\hat{A}_k - K_{s_k} C)\hat{x}_k + \hat{B}_k \bar{u}_k + K_{s_k} y_k \\ P_{s_{k+1}} &= (\hat{A}_k - K_{s_k} C) P_{s_k} \hat{A}_k^T + Q_s \end{aligned} \tag{33}$$

as derived in [7], we are able to get estimates $\hat{\varphi}_k$, $\hat{\dot{\varphi}}_k$ and $\hat{\tau}_{d_k}$, which are used in the control law described in sec. V.

In our approach we separated state and parameter estimation in a RLS parameter estimator (cf. e.g. [7], [9]) and a Kalman filter for state estimation. An alternative would be the joint parameter and state estimation as provided for instance by Bootstrap Algorithms as suggested e.g. in [10], [7] and [11]. We however decided to separate parameter and state estimaton for three reasons:

First of all there are less parameters to estimate in our approach compared to a Bootstrap Algorithm, since this algorithm estimates simultaneously plant parameters and Kalman gain K_s for state estimation. Therefore, to achieve parameter convergence, the plant input signal I can be persistently exciting of a lower order in our approach compared to a Bootstrap Algorithm.

Secondly, since (7) can be written as a linear regression, it is suitable for an RLS-type parameter estimator. For a Bootstrap Algorithm an parameter estimator based on pseudo linear regression would be needed, e.g. Extended Least Squares (ELS). The convergence properties of these estimators are more restrictive compared to an RLS algorithm.

Thirdly we filter RLS inputs u_k and φ_k, as suggested in [9], to suppress noise and to use only informative data for parameter estimation. In our approach, the parameter estimator is independent from state estimation, therefore the filter is not part of the closed control loop. Due to combined state and parameter estimation the Bootstrap Algorithm in contrary would be part of the control loop. Therefore the filter becomes part of the control loop, too, and filter dynamics may deteriorate closed loop dynamics.

V. Controller

Using state estimates from (33) and disturbance feed forward (24) together with reference input r, we are able to formulate the following control law:

$$\begin{aligned} u_k &= r_k - k_{1_k}\hat{\varphi}_k - k_{2_k}\dot{\hat{\varphi}}_k + \frac{\hat{\tau}_{d_k}}{k_m} \\ &\quad + \frac{\hat{\tau}_{c_k}}{k_m} sgn(\dot{\hat{\varphi}}_k) + \frac{\hat{\tau}_{u_k}}{k_m} cos(\hat{\varphi}_k) \end{aligned} \tag{34}$$

With the control law (34) applied to plant (5) and using z-Transformation we derive a second order closed loop system with characteristic equation

$$\begin{aligned} z^2 &+ \frac{1}{J}(Td + k_m T k_2 - 2J)z \\ &+ \frac{1}{J}(J - Td - k_m T k_2 + k_m T^2 k_1) = 0 \end{aligned} \tag{35}$$

Feedback gain k_1 and k_2 are determined by comparison of coefficients with the desired 2^{nd} order closed loop characteristic polynomial

$$z^2 + 2(\zeta\omega_0 T - 1)z + (\omega_0^2 T^2 - 2\zeta\omega_0 T + 1) = 0 \tag{36}$$

with closed loop natural frequency ω_0 and damping ζ. After replacing the plant parameters with their estimates we derive:

$$k_1 = \hat{J}\omega_0^2/k_m, \quad k_2 = (2\zeta\omega_0\hat{J} - \hat{d})/k_m \tag{37}$$

To determine ω_0 we use the design relations for dominant second order closed loop poles given in [12].

$$\omega_0 = 4.6/(\zeta t_s) \tag{38}$$

with settling time t_s and damping ζ. Damping is chosen $\zeta > 1$ to avoid overshoot. Acceleration time t_a for angular position φ depends on

$$\varphi = \frac{1}{2}\ddot{\varphi}t_a^2 \Leftrightarrow t_a = \sqrt{2\varphi/(k_m I)}\sqrt{J} \tag{39}$$

Since t_a is a function of $\sqrt{J}$ we have chosen

$$t_s = \lambda\sqrt{\hat{J}} \tag{40}$$

as adjustment rule for t_s, where λ is an empirically derived constant, that offers a good compromise between step response time and actuator saturation.

The platform's task is either to track objects or to conduct fast saccades. Therefore the reference r is designed to track the desired yaw angle φ_{ref} up to a ramp signal without steady state error. Thus r is a linear combination of φ_{ref} and its time derivative $\dot{\varphi}_{ref}$

$$r = w_1\varphi_{ref} + w_2\dot{\varphi}_{ref} \tag{41}$$

with gains w_1 and w_2. Using discretization (6) and applying z-Transform we derive the discrete time reference signal

$$r(z) = (w_1 + \frac{z-1}{T}w_2)\varphi_{ref} \tag{42}$$

Defining the tracking error

$$\varphi_{ref}(z) - \varphi(z) = \left(1 - \frac{\varphi(z)}{\varphi_{ref}(z)}\right)\varphi_{ref}(z) = e(z)\varphi_{ref}(z) \tag{43}$$

and calculating the steady state error using the final value theorem according to [5] we get

$$\lim_{z\to 1}\left((z-1)e(z)\frac{Tz}{(z-1)^2}\right) = \lim_{z\to 1}\left(e(z)\frac{Tz}{z-1}\right) \tag{44}$$

The nominator polynomial of $e(z)$ is

$$(z-1)^2 + q_1 z + q_2 \tag{45}$$

with coefficients

$$\begin{aligned} q_2 &= \frac{T}{J}(-d - k_m k_2 + T k_m k_1 + k_m w_2 - T k_m w_1) \\ q_1 &= \frac{T}{J}(d + k_m k_2 - k_m w_2) \end{aligned} \tag{46}$$

If w_1 and w_2 are as follows

$$w_1 = k_1, \quad w_2 = k_2 + \frac{\hat{d}}{k_m} \tag{47}$$

q_1 and q_2 equal zero, provided $\hat{d}$ approaches d. Then steady state tracking error (44) will also be zero and therefore ramp following without steady state tracking error is established.

VI. Stability Considerations

In this section we want to demonstrate that the stability proof given in [7] for an adaptive pole placement algorithm can be applied to our control law design. Note first, that using equation (24) and defining controller gain

$$K_c = (k_1, \quad k_2, \quad -k_m^{-1}, \quad 0)^T \tag{48}$$

control law (34) can be rewritten as

$$\bar{u}_k \quad = \quad r_k - K_{c_k}\hat{x}_k \tag{49}$$

From equation (49) and state estimator (33) we get

$$\begin{aligned} \hat{x}_{k+1} &= (\hat{A}_k - \hat{B}_k K_{c_k} - K_{s_k} C)\hat{x}_k + \hat{B}_k r_k + K_{s_k} y_k \\ \bar{u}_k &= -K_{c_k}\hat{x}_k + r_k \end{aligned} \tag{50}$$

After applying z-Transform to (50), we can derive the two transfer functions $\bar{u}(z)/r(z)$ from reference input $r(z)$ to controller output $\bar{u}(z)$ and $\bar{u}(z)/y(z)$ from plant output $y(z)$ to controller output $\bar{u}(z)$. As described in [12] we obtain

$$\frac{\bar{u}(z)}{r(z)} = \frac{det\begin{pmatrix} zI-\hat{A}+\hat{B}K_c+K_sC_d & -\hat{B} \\ -K_s & 1 \end{pmatrix}}{det(zI-\hat{A}+\hat{B}K_c+K_sC_d)} = \frac{\hat{M}(z)}{\hat{L}(z)} \tag{51}$$

and

$$\frac{\bar{u}(z)}{y(z)} = \frac{det\begin{pmatrix} zI-\hat{A}+\hat{B}K_c+K_sC & -K_s \\ -K_s & 0 \end{pmatrix}}{det(zI-\hat{A}+\hat{B}K_c+K_sC_d)} = \frac{\hat{P}(z)}{\hat{L}(z)} \tag{52}$$

Thus having controller polynomials $\hat{M}(z)$, $\hat{P}(z)$ and $\hat{L}(z)$ as well as state space model (31) and (32) rewritten in polynomial form $A_p(z)y(z) = B_p(z)\bar{u}(z)$, the closed loop transfer function $y(z)/r(z)$ can be written as

$$\frac{y(z)}{r(z)} = \frac{B_p(z)\hat{M}(z)}{A_p(z)\hat{L}(z) + B_p(z)\hat{P}(z)} \tag{53}$$

Since we used state space design techniques to derive the control law (50), the desired closed loop characteristic polynomial $A^*(z)$ is as follows

$$A^*(z) = det(zI - \hat{A} + \hat{B}K_c) \cdot det(zI - \hat{A} + K_sC) \tag{54}$$

with desired closed loop poles $det(zI - \hat{A} + \hat{B}K_c)$ resulting from state feedback control law as defined in equation (49) and $det(zI - \hat{A} + K_sC)$ as characteristic polynomial of the state estimator (33). K_c is chosen such that equation (36) is satisfied and K_s is the Kalman gain derived from (33). As a result of the proof in [7, sec. 6.5] the closed loop characteristic polynomial of transfer function (53) tends to the desired closed loop characteristic polynomial $A^*(z)$:

$$A_p(z)\hat{L}(z) + B_p(z)\hat{P}(z) \rightarrow A^*(z) \text{ for } t \rightarrow \infty \tag{55}$$

The proof establishes:

$$\begin{aligned} &(i) \quad \bar{u}(z), y(z) \text{ bounded} \\ &(ii) \quad \lim_{z\rightarrow 1}(z-1)\left(A^*(z)y(z) - \hat{B}_p(z)\hat{M}(z)r(z)\right) = 0 \end{aligned} \tag{56}$$

for time invariant plant parameters if $\hat{A}_p(z)$, $\hat{B}_p(z)$, $\hat{L}(z)$, $\hat{P}(z)$ and $\hat{M}(z)$ are bounded. Furthermore, if the plant is stable, the stability proof can be extended to the practically important case that $\bar{u}(z)$ saturates [13]. Note that convergence of the estimated parameters to the true plant parameters is not necessary for the proof.

Plant parameters are considered time invariant since the controller is switched off during camera exchange. Furthermore the plant is stable. $\hat{A}_p(z)$ and $\hat{B}_p(z)$ are bounded due to the properties of the RLS-algorithm (12) to (15) [7, Lemma 3.3.8]. The Kalman filter (33) is stable if $(\hat{A}, C)$ is detectable [7]. Since $(\hat{A}, C)$ is observable it is also detectable and thus (33) is stable which implies that K_s is bounded. $\hat{A}_p(z)$ and $\hat{B}_p(z)$ are bounded, thus $\hat{J}$ and $\hat{d}$ are bounded either. Therefore equation (37) results in bounded K_c such that the desired closed loop characteristic equation (36) is satisfied. It follows that all coefficients in (51) and (52) are bounded, which again implies that $\hat{L}(z)$, $\hat{P}(z)$ and $\hat{M}(z)$ are bounded polynomials. Since the preconditions for the stability proofs in [7] and [13] are met, we can conclude that the presented controller is stable in the above sense (56).

VII. Experimental Results

To test the validity of our approach, we conducted several experiments with two changing configurations of the camera platform. We used the configurations shown in Figure 1 with two and four cameras called 2c- and 4c-configuration, respectively. No pitch camera was used for this test. To test both step responses and the tracking of a position ramp, we switched the reference signal repeatedly between a square signal with amplitude 15° and $2s$ cycle time and a position ramp with slope $5°/s$ and $10s$ cycle time. Figure 2 depicts

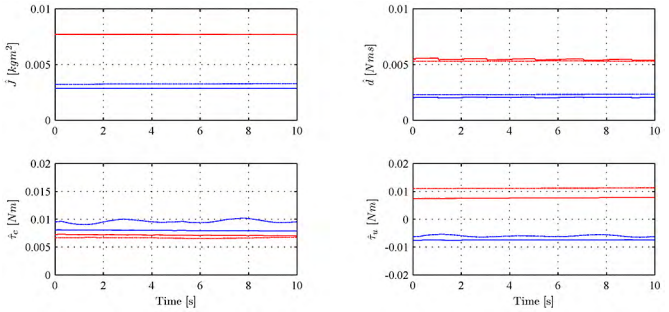

Fig. 2. Estimated plant parameters: The red line corresponds to the 4c-, the blue line to the 2c-configuration. Solid lines correspond to step responses and dash-dotted lines to position ramp tracking.

the estimated plant parameters. Rough approximations of the real inertias ($J_{2c} \approx 0.002\ kgm^2$, $J_{4c} \approx 0.006\ kgm^2$) indicate that the estimated inertias $\hat{J}$ converge towards realistic values. Estimated viscous friction coefficient $\hat{d}$ increases with the number of the attached cameras. The estimated Couloumb friction coefficient $\hat{\tau}_c$ seems to be independent from the platform configuration. $\hat{\tau}_u$, resulting from unbalanced mass, changes its sign with the change from the 2c- to the 4c-configuration. For the 2c-configuration pitch axis encoder is outweighing pitch axis drive, resulting in a negative $\hat{\tau}_u$ (Fig.1(b)). For the 4c-configuration the two cameras on the side of the pitch axis drive are equipped with larger lenses,

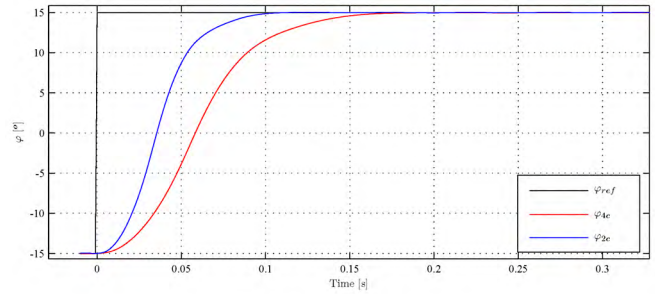

(a) Step response

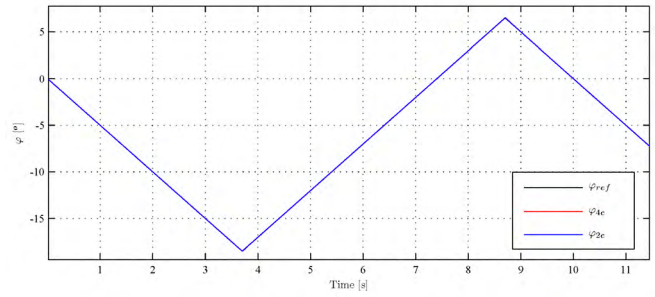

(b) Tracking a position ramp

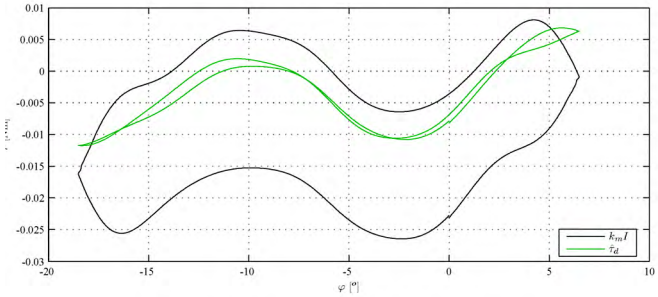

(c) Disturbance rejection (2c-configuration)

Fig. 3. Control performance

compared to the two cameras on the opposite side, leading to a positive sign of $\hat{\tau}_u$ (Fig.1(b)). Since these are closed loop experiments, we cannot expect, that the estimated parameters approach the true values of the plant parameters. Moreover, the estimates depend on the kind of experiment conducted (step response or position ramp). However, the estimates converge to constant values. This indicates, that the stability considerations in section VI are valid and therefore our control objectives can be achieved without parameter convergence. In Figure 3(a) the step responses for the two configurations are shown. The step response of the 4c-configuration is slower compared to the 2c-configuration. This is due to higher inertia and the corresponding adjustment of closed loop dynamics. The tracking of a position ramp seems not to be affected by the two different platform configurations (Fig. 3(b)). Figure 3(c) depicts the effects of disturbance feedforward (24) while tracking a position ramp (2c-configuration only). It shows the plant reference torque $k_m I$ over position φ in black. This is a measure for the real disturbance torque, since in the undisturbed case at constant velocity $k_m I$ equals zero. The disturbance torque comprises Coulomb friction torque, offset torque resulting from unbalanced mass and torque ripple that originates from the drive bearings. The hysteresis of $\pm 0.01 Nm$ between the two black lines is a measure for the friction torque. Without unbalanced mass disturbance torque would be symmetric to the zero torque line. Therefore the displacement of $-0.01 Nm$ is a measure for the disturbance torque resulting from unbalanced mass. Estimated disturbance torque $\hat{\tau}_d$ is shown in green. The estimated offset torque is approximately half of the size of the real offset torque. The estimated friction torque is nearly zero and the estimated torque ripple corresponds to the real torque ripple. This indicates, that the disturbance feedforward (24) compensates effectively for friction (τ_c) and offset torque (τ_u).

VIII. Conclusion

In this paper a multi focal camera platform is presented together with its motion controller. The platform is designed for easy exchange of the cameras while preserving extrinsic camera parameters for later reuse of a platform configuration. The possibility of altering platform configurations implies the need for an adaptive motion controller. The adaptive state space control algorithm proposed in this paper meets the control objectives of fast saccades and tracking of a position ramp. Moreover it was shown that the control algorithm is stable. But noting that the step responses in figure 3(a) are not perfectly symmetric, there might be the possibility to further speed up the step responses by means of an improved controller. The investigation of the achievable repeat accuracy concerning the extrinsic camera parameters is also left to future research.

References

[1] E. D. Dickmanns, "An advanced vision system for ground vehicles," in *Proceedings of the 1st International Workshop on 'In-Vehicle Cognitive Computer Vision Systems'*, Graz, Austria, April 2003.

[2] ——, *Dynamic Vision for Perception and Control of Motion*. London: Springer, 2007.

[3] K. Kühnlenz, M. Bachmayr, and M. Buss, "A Multi-Focal High-Performance Vision System," *Proceedings of the 2006 IEEE International Conference on Robotics and Automation*, pp. 150–155, 2006.

[4] K. Kühnlenz, "Aspects of Multi-Focal Vision," Dissertation, Technische Universität München, München, 2006.

[5] J. Schiehlen, "Kameraplattformen für aktiv sehende Fahrzeuge," Dissertation, Universität der Bundeswehr München, 1995.

[6] C. Canudas, K. J. Åström, and K. Braun, "Adaptive Friction Compensation in DC-Motor Drives," *IEEE Journal of Robotics and Automation*, vol. RA-3, No. 6, pp. 681–685, 1987.

[7] G. C. Goodwin and K. S. Sin, *Adaptive Filtering Prediction And Control*, ser. Information and System Sciences, T. Kailath, Ed. Engelwood Cliffs, New Jersey 07632: Prentice-Hall, Inc, 1984.

[8] A. Ramasubramanian and L. R. Ray, "Comparison of EKBF-based and Classical Friction Compensation," *Journal of Dynamic Systems, Measurement, and Control*, vol. 129, pp. 236–242, 2007.

[9] K. J. Åström and B. Wittenmark, *Adaptive Control*, ser. Control Engineering. New York: Addison-Wesley Publishing Company, 1989.

[10] A. Gambier and Y. Y. Nazaruddin, "Multivariable State-space Adaptive Control," *Automatisierungstechnik*, vol. 11/53, pp. 537–545, 11 2005.

[11] M. S. Ahmed and N. Sait, "State-space adaptive control through a modified bootstrap algorithm for parameter and state estimation," in *IEEE Proceedings*, vol. 136, no. 5, 1989, pp. 215–224.

[12] G. F. Franklin, J. D. Powell, and A. Emami-Naeini, *Feedback Control of Dynamic Systems*, 4th ed. Upper Saddle River, New Jersey: Prentice Hall, 2002.

[13] D. Y. Abramovitch and G. F. Franklin, "On the Stability of Adaptive Pole Placement Controllers with a Saturating Actuator," *IEEE Transactions on Automatic Control*, vol. 35, no. 3, pp. 303–306, March 1990.